Ab Initio Molecular Orbital Studies on the Chemiluminescence of 1,2-Dioxetanes

Chizuko Tanaka and Jiro Tanaka*

Department of Chemistry, Faculty of Science, Kanagawa University, Hiratsuka, 259-1293, Japan

Received: September 1, 1999; In Final Form: December 14, 1999

The mechanism of chemiluminescence of 1,2-dioxetane (DO) and 3,3,4,4-tetramethyl-1,2-dioxetane (TMDO) are investigated by the ab initio molecular orbital calculation. The rate-determining step of the chemiluminescent reaction is the O−O bond breaking to form the biradicals. The potential energies along the reaction path are calculated by uB3LYP and uB3P86 methods with 6-31+G(d); the calculated potential barriers are in reasonable agreement with experimental activation energies. An overview of the potential surfaces for overall reaction is obtained. The intersystem crossing mechanism from the singlet biradical to the triplet state is investigated, and the reaction path is followed to the $^3(n\pi^*)$ excited states of the carbonyl group of respective fragment molecules. The mechanism of promotion to the $^1(n\pi^*)$ excited state of formaldehyde is investigated by the MCSCF method on DO. The reaction rates and the yield of chemiluminescence are discussed by the RRKM theory of unimolecular reaction.

1. Introduction

Chemiluminescence of dioxetanes is a process in which chemical energy is converted to light due to breaking and making of bonds in the reaction. The change of the electronic structure during the reaction is particularly interesting from a view of producing an excited state through chemical reaction.

Dioxetanes are prototypes of chemiluminescent molecules. By heating they smoothly decompose into two carbonyl compounds, one of which has a good chance of being formed in an excited electronic state. A lot of papers have been published on the experimental and theoretical studies of chemiluminescence of 1,2-dioxetane (DO),[1−3] and it is established that the emission from the triplet state is dominant. The biradical mechanism has been considered[4−7] for the thermal decomposition of 1,2-dioxetane. On substituted dioxetanes and dioxetanones with easily oxidized groups, the electron or the charge transfer mechanism has been proposed to account for the high yields of the singlet excited state.[8,9] Accordingly, the detailed analysis of the electronic structure of DO is important to understand the two different types of chemiluminescent processes. Recently, attention to chemiluminescence has been growing as more efficient chemiluminescent molecules have been synthesized.[10−13]

Theoretical studies have continued to elucidate the reaction path and the energetics of the dissociation process. In particular, Reguero, Bernardi, and Robb et al.[14] found structures of transient species appearing in the dissociation reaction by the ab initio MCSCF calculation. Wilson and Halpern[15] and Vasil'ev[16] used a semi-empirical method to find the reaction path of decomposition of DO and confirmed the earlier work of Goddard et al.[7] Yamaguchi et al.[17] used the uMP2 method to calculate the energies of biradical states for the decomposition of DO.

A series of methyl-substituted dioxetanes were synthesized by Adam and Baader,[18] and it was found that the stabilities and quantum yields of chemiluminescence were significantly affected by the methyl group substitution. Infrared lasers were used to investigate the dynamics of chemiluminescence of 3,3,4,4-tetramethyl-1,2-dioxetane (TMDO); a short-lived X-emission band was found, but its origin has not yet been clarified.[19−21]

Recently, the accuracy and utility of the ab initio MO calculation have been improved by the introduction of the DFT method.[22−24] We used Becke's three-parameter hybrid method to calculate the optimized structures and energies of transient species in thermal decomposition of DO and TMDO. We also used the MCSCF method[14] to study the mechanism of the singlet excited (S_1) state being formed. The intersystem crossing mechanism is also investigated. The reaction rates of the thermal dissociation and the yield of chemiluminescence are discussed by the RRKM theory.

2. Methods

All calculations were performed with the Gaussian 94 and 98 programs.[24] The main part of the calculations includes the geometry optimizations, vibrational frequencies, and intrinsic reaction coordinate (IRC) calculations for the structures on the reaction path. The optimized geometries were characterized with the use of their vibrational frequencies.

Becke's three-parameter hybrid method (uB3LYP)[22] with the basis functions 6-31+G(d) was used for the species either in the ground state (S_0) and the triplet state (T_1). We also used the uB3P86/6-31+G(d)[23] to confirm the energies of several important species. To produce the unrestricted guess orbitals for the S_0 state, the HOMO and the LUMO were mixed so as to destroy spatial symmetries in $\alpha-\beta$ spin orbitals. The following reaction path was performed with the IRC program using mass-weighted internal coordinates with a step size of 0.1 bohr $(\text{amu})^{1/2}$ unit. The MCSCF was used to find the S_0/T_1 and the S_0/S_1 intersections, to calculate the energies of spin−orbit coupling, and to calculate IRC curves for the S_0, T_1, and S_1 states.

The accuracy of the B3LYP and B3P86 methods compared to G2 theory has been discussed for many molecules.[22,25,26] Politzer and Seminario[27] have calculated the bond dissociation energies of H_3C-NO_2, H_3C-OH, and H_3C-CN by several hybrid DFT methods with different basis sets. Most of the calculated results are in reasonable agreement with the experiment (within 4 kcal/mol). These calculations are carried out by

10.1021/jp9931004 CCC: $19.00
Published on Web 02/18/2000

TABLE 1: Yield of Chemiexcitation of 3,3,4,4-Tetramethyl-1,2-Dioxetane and 1,2-Dioxetane[18]

compounds	triplet	singlet
3,3,4,4-tetramethyl-1,2-dioxetane	0.35	2.5×10^{-3}
1,2-dioxetane[a]	0.0024	3.1×10^{-6}

[a] The values for 1,2-dioxetane may suffer some error because they were estimated by fluorescence of 9,10-dibromoanthracene (DBA) through energy transfer from the T_1 of formaldehyde to the T_2 of DBA, which may not be 100% efficient because the T_2 state is higher by 2 kcal/mol than the T_1 state. We thank referees for commenting on this point.

finding energy differences between the reactants and the products. On the other hand, energy changes in the same molecule—for example, rotational barriers—are calculated with much better accuracy (within less than 0.5 kcal/mol) because little change in molecular and electronic structure is concerned.

The calculations were carried out mainly with the computers at Kanagawa University (Hiratsuka campus) and partly in the computation center of the Institute for Molecular Science (IMS) in Okazaki.

3. Summary of Experimental Results

Experimental features on thermolysis, energetics, and yields of chemiexcitation are summarized as follows.[3,4,18,19,20,21]

1. Methylsubstituted 1,2-dioxetanes need thermal energy to form the activated complex; the activation enthalpies are 22 kcal/mol for DO and 25 $\sim$ 27 kcal/mol for methylsubstituted DOs, depending on the number of methyl groups.

2. The activated complex dissociates to the triplet or the singlet excited fragments and ground state of formaldehyde, acetaldehyde, or acetone.

3. The S_1 $n\pi^*$ excited state of acetone was estimated at 85 kcal/mol and the T_1 $n\pi^*$ state at 80 kcal/mol. The values for formaldehyde are 80 kcal/mol and 72 kcal/mol for the S_1 and the T_1 states, respectively. Taking the sum of thermochemical data on the heat of reaction and the activation enthalpies, the energy of the activated complex of DO is estimated as 74 $\sim$ 77 kcal/mol; this is not sufficient to excite for the S_1 state. The activated complex of TMDO has 94 kcal/mol, which is sufficient for the T_1 and the S_1 excitation of acetone.

4. The triplet excitation yields are two orders of magnitude larger than those of the singlet state in both DO and TMDO. The triplet yield of TMDO is 0.35, while the value for DO is smaller by two orders of magnitude (Table 1).

5. By the infrared laser excitation to the overtones of the C−H vibration of TMDO, the chemiluminescence starts by the rate which depends on the energy of the excitation. Immediately after the excitation, a blue-shifted emission (X band) was found before the triplet emission of acetone became apparent. The origin of the X band has not yet been assigned. These characteristics will be discussed in the following section.

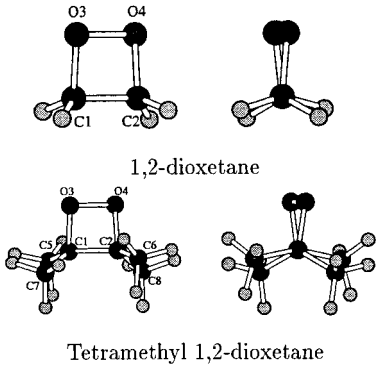

Figure 1. Perspective of 1,2-dioxetane and 3,3,4,4-tetramethyl-1,2-dioxetane molecules.

4. Results and Discussion

4.1. (a) Stable Structures of DO and TMDO. The optimized geometries of the stable conformation (A) of DO and TMDO are shown in Figure 1. The geometrical parameters of the DO ring are listed in Table 2, with the data of two DO derivatives by the X-ray crystal structural analysis.[28,29] The agreement between the calculated and the experimental values is satisfactory. The C_1-C_2 bond lengths show the effect of bulky substituent groups; the dihedral angles show the same effect, except in DMTOH, where the C_1-C_2 bond of the DO ring is shared by the tetrahydrofuran ring. The square rings of DO and TMDO at point A are not planar; consequently, they have their antipodes. The transition state between them (denoted 0 in Table 3) has a planar ring, where the barrier heights are only 0.09 and 0.69 kcal/mol for DO and TMDO, respectively.

To clarify the electronic process of producing the excited state by the bond rupture, the changes of MOs during the reaction are illustrated in Figure 2, where the coordinate axis is the same as in Scheme 1. In state (A), the HOMO (No. 16) and the next HOMO (No. 15) comprise the nonbonding orbitals, the $O_3$2py and the $O_4$2py, which are antisymmetrically combined in the 16th MO and symmetrically combined in the 15th MO. The 11th and the 14th MOs constitute the σ bonding orbitals of the C_1-C_2 and the O_3-O_4 bonds, which are described by the O_4-2pz $-$ $O_3$2pz and the $C_1$2pz $-$ $C_2$2pz orbitals. The 17th MO is the O_3-O_4 antibonding orbital, $O_3$2pz $+$ $O_4$2pz, which is unoccupied in state A. If DO is decomposed concertedly from A, keeping the symmetry of MOs, the two formaldehyde molecules produced are in the $\pi - \pi^*$ excited states; this is not allowed energetically, as has been discussed by Woodward-Hoffman's rule.

TABLE 2: Bond Lengths and Angles in the 1,2-Dioxetane ring

	optimized geometries					
	DO		TMDO		X-ray analysis	
compounds	B3LYP[c]	B3P86[c]	B3LYP[c]	B3P86[c]	AADO[a]	DMTOH[b]
r(C1−C2) Å	1.521	1.515	1.558	1.549	1.549	1.584
r(C1−O3) Å	1.455	1.445	1.471	1.461	1.476	1.485
r(C2−O4) Å	1.455	1.445	1.471	1.461	1.474	1.459
r(O3−O4) Å	1.492	1.476	1.488	1.473	1.491	1.497
∠C2−C1−O3°	88.87	88.61	87.46	87.19	86.9	87.1
∠C1−C2−O4°	88.87	88.61	87.46	87.18	86.8	89.0
∠O4−C2−C1−03°	11.54	11.96	16.39	17.30	21.3	7.7

[a] AADO: adamantylideneadamantane-1,2-dioxetane.[28] [b] DMTOH: 1-aryl-5-(9-methylfluorene-9-yl)-4,4-dimethyl-2,6,7-trioxabicyclo[3,2,0]heptane.[29] [c] Basis set is 6-31+G(d).

TABLE 3: Energies and Skeletal Part of Geometrical Parameters[a] for Energy Minima and Transition States along the Reaction Path of Thermolysis of 1,2-Dioxetane into Two Formaldehyde Molecules in the Ground State (S_0): uB3LYP/6-31+G(D)//uB3LYP/6-31+G(D)

a. Ground State (S_0)

species	ts 0	min A	ts B	S_0/T_1	min K1	ts G1	min K2	ts D1	min F	ts P1	min K3	ts D2
total energy *E*												
Hartree (−228. +)	−0.933325	−0.933466	−0.901267	−0.903521	−0.922622	−0.922581	−0.922844	−0.922655	−1.021818	−0.921446	−0.924142	−0.923591
Δ*E* kcal/mol	0.09	0.00	20.21	18.79	6.80	6.83	6.67	6.78	−55.44	7.54	5.85	6.20
zero-point energy Hartree (ZPE)	0.062001	0.062233	0.058540		0.055471	0.053892	0.056065	0.054533	0.055095	0.055411	0.055889	0.054931
Δ(*E* + ZPE) kcal/mol	−0.06	0.00	17.89		2.56	1.60	2.79	1.95	−59.92	3.26	1.87	1.61
r(C1−C2) Å	1.523	1.521	1.519	1.522	1.540	1.534	1.545	1.581	3.685	1.550	1.546	1.600
r(C1−O3) Å	1.455	1.455	1.427	1.411	1.367	1.370	1.366	1.354	1.213	1.365	1.365	1.348
r(C2−O4) Å	1.455	1.455	1.427	1.411	1.367	1.370	1.366	1.354	1.213	1.365	1.365	1.348
r(O3−O4) Å	1.491	1.492	1.996	2.145	3.028	3.073	3.137	3.086	3.513	3.477	3.647	3.598
∠C2−C1−O3	89.37	88.87	97.17	100.12	114.94	114.97	114.14	112.24	66.53	115.11	114.22	111.17
∠C1−C2−O4	89.37	88.87	97.17	100.12	114.94	114.96	114.13	112.24	66.53	115.10	114.22	111.17
∠O4−C2−C1−O3	0.00	−11.54	−28.04	−30.42	−67.96	−73.11	−83.42	−82.59	−180.00	−123.74	−179.92	−180.00

b. Triplet (T_1) Energies for the Same Geometries with Those of Energy Minima and Transition States in Singlet Ground State (S_0)

species	ts 0	min A	ts B	S_0/T_1	min K1	ts G1	min K2	ts D1	min F	ts P1	min K3	ts D2
total energy *E*												
Hartree (−228. +)		−0.827337	−0.897531	−0.903428	−0.922913	−0.922449	−0.923651	−0.923278		−0.922013	−0.924680	−0.923714
Δ*E* kcal/mol		66.60	22.55	18.85	6.62	6.91	6.16	6.39		7.19	5.51	6.12

[a] The unit of angle is degree.

Figure 2. Change of molecular orbitals of 1,2-dioxetane along the reaction path. The top three rows are MOs (16−14) of the S_0 state. The bottom four rows are MOs (17−14) of the T_1 state. The symbols of states are the same as those of Scheme 1 and Tables 3−4.

SCHEME 1: Reaction Pathway of 1,2-Dioxetane to Two Formaldehyde Molecules[a]

[a] The drawings are the projection of the optimized geometries onto the $O_3-C_1-C_2$ plane. The *z*-axis is set to the C_1-C_2 bond direction and the *xz* plane is on the $O_3-C_1-C_2$ plane. White circles illustrate oxygen atoms. Thermolytic process is shown on the right and the chemiluminescent process is on the left. The symbols for the potential maxima are underlined.

(b) Thermal Decomposition of DO in the S_0 State. DO thermally decomposes easily. The energy minima and transition states of the S_0 and the T_1 states found along the reaction path are illustrated in Scheme 1; the drawings are projections of optimized geometries to the $O_3-C_1-C_2$ plane. White circles refer to O atoms. The total energies, zero-point energies, and optimized geometrical parameters for these points are shown in Tables 3 and 4. Figures 3 and 4 show the results of the reaction path obtained by the IRC for the gauche and trans routes, respectively. Potential energies are given in relative values to point A, except as otherwise stated.

TABLE 4: Energies and Skeletal Part of Geometrical Parameters[a] for Energy Minima and Transition States along the Reaction Path of Thermolysis of 1,2-Dioxetane into Two Formaldehyde Molecules in the Triplet State (T_1): uB3LYP/6-31+G(d)//uB3LYP/6-31+G(d)

species	min J1	ts H1	min J2	ts Q1	min Z	ts P2	min J3	ts H2	min J4	ts Q2
total energy Hartree(−228. +)	−0.923097	−0.922490	−0.923755	−0.909299	−0.912222	−0.922089	−0.924728	−0.924137	−0.924242	−0.910333
ΔE kcal/mol	6.51	6.89	6.09	15.16	13.33	7.14	5.48	5.85	5.79	14.52
zero-point energy Hartree (ZPE)	0.056063	0.054244	0.056566	0.053042	0.051753	0.055759	0.056253	0.055557	0.056537	0.053385
$\Delta(E + \text{ZPE})$ kcal/mol	2.63	1.87	2.54	9.40	6.75	3.08	1.73	1.66	2.21	8.96
r(C1−C2) Å	1.554	1.533	1.555	2.286	2.977	1.556	1.552	1.586	1.602	2.270
r(C1−O3) Å	1.360	1.371	1.361	1.232	1.213	1.361	1.362	1.355	1.349	1.234
r(C2−O4) Å	1.360	1.371	1.361	1.296	1.307	1.361	1.362	1.350	1.346	1.299
r(O3−O4) Å	3.007	3.050	3.146	3.656	4.574	3.494	3.637	3.585	3.563	3.906
∠C2−C1−O3	114.65	115.14	113.61	105.46	97.25	114.64	113.74	108.20	106.06	102.47
∠C1−C2−O4	114.64	115.14	113.61	114.32	134.40	114.64	113.74	113.39	113.16	115.76
∠O4−C2−C1−O3	−66.03	−70.07	−86.28	−103.34	−180.00	−128.47	−179.93	−175.77	−179.95	−179.99

[a] The unit of angle is degree.

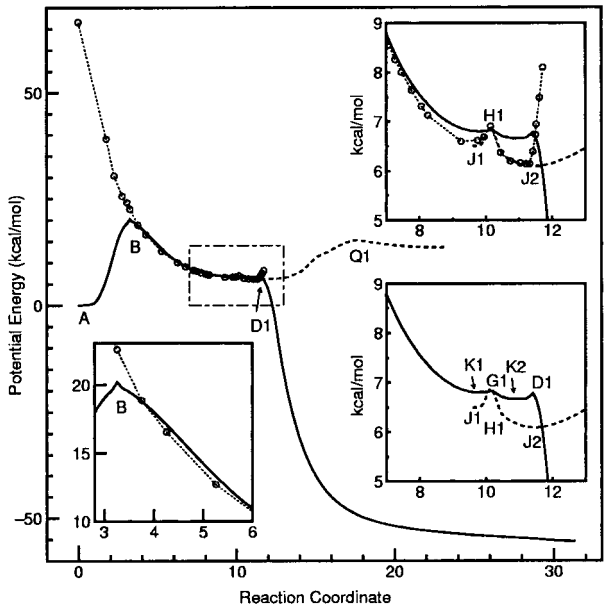

Figure 3. Potential energy curves of the decomposition of 1,2-dioxetane to two formaldehyde molecules through gauche route. The solid line is the IRC curve of the S_0 state and the broken line is the IRC curve of the T_1 state. Circles are calculated values of the T_1 state with the geometries of the S_0 state on the IRC. The insets are details of the potential energy curves; the top right shows the T_1 surface is below the S_0 surface. The bottom left shows the T_1 surface intersects with the S_0 surface and is below the S_0 surface after the intersection. The bottom right illustrates the symbols of states shown in Scheme 1 and Tables 3−4.

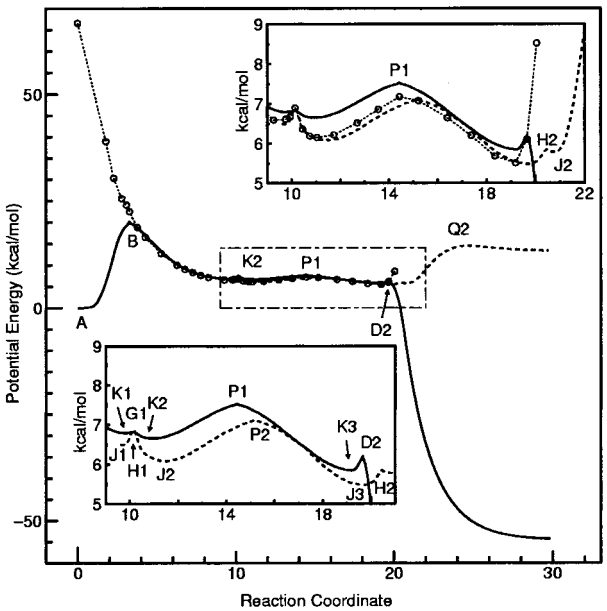

Figure 4. Potential energy curves of the decomposition of 1,2-dioxetane to two formaldehyde molecules through the trans route. The thick solid line is for the S_0 state and the broken line is for the T_1 state. Circles show the calculated energies of the T_1 state with the geometries of the S_0 state. The upper inset illustrates the T_1 surface is below the S_1 surface in the biradical region. The lower inset shows symbols of states shown in Scheme 1 and Tables 3−4.

As shown in these figures, the highest energy point on the reaction path is B; accordingly, the process A → B is the rate-determining step. The geometry of B is characterized by the dihedral angle τ, $\tau = \angle O_4{-}C_2{-}C_1{-}O_3$, 28°, and the $O_3{-}O_4$ distance of 2.00 Å. The potential barrier is 20.2 kcal/mol by the uB3LYP/6-31+G*. Slightly larger values are obtained by the uB3P86/6-31+G* and the CCSD(T)/6-31G*, as shown in

TABLE 5: Activation Energies for the O−O Bond Breaking; Total Energies, E_A and E_B, of the Initial and Transition States

	E_A (Hartree)	E_B (Hartree)	ΔE [a] (kcal/mol)	$\Delta(E + \text{ZPE})$[b] (kcal/mol)	exptl. (kcal/mol)
DO					
uB3LYP[c]	−228.933466	−228.901267	20.2	17.9	18.9[3]
uB3P86[d]	−229.502016	−229.465299	23.0	20.7	22.7[18]
uCCSD(T)[e]	−228.298562	−228.263844	21.8	19.5	21.5[4]
TMDO					24.9[3]
uB3LYP[c]	−386.217914	−386.181234	23.0	21.1	27.8[18]
uB3P86[d]	−387.373961	−387.332837	25.8	23.8	24.7[4]

[a] The energy difference between the initial state A and the transition state B. [b] The energy difference including the zero point correction (ZPE) calculated with method c. The scale factor is 1.0. [c] uB3LYP/6-31+G(d)//uB3LYP/6-31+G(d). [d] uB3P86/6-31+G(d)//uB3P86/6-31+G(d). [e] uCCSD(T)/6-31G(d)//uB3LYP/6-31+G(d).

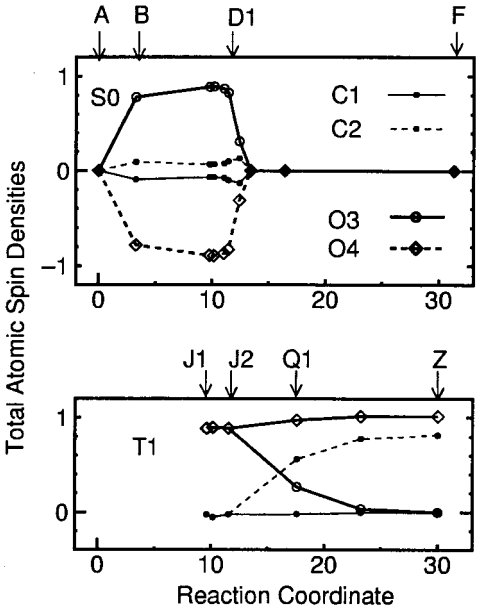

Figure 5. Change of atomic spin densities along the reaction coordinates. In the singlet biradical region, B−D_1 (gauche), the positive and negative spin densities are found on O_3 and O_4, respectively. After the C_1−C_2 bond breaking through the point Q_1, the triplet spin state appears on the C_2 and the O_4 atoms. The trans route shows similar changes of atomic spin densities.

Table 5. The agreement with experimental activation energies is satisfactory, and further discussion will be given in the last section.

The transition state (B) is a biradical whose total atomic spin densities on the O_3 and the O_4 atoms are 0.78 and −0.78, respectively (Figure 5). We will explain the electron configuration of the biradical with the MOs shown in Figure 2. By elongating the O_3−O_4 bond, the antibonding σ^* orbital, $O_3$2pz + $O_4$2pz, is mixed with the σ bonding orbital (the 14th MO of A) to give localized spin orbitals on the O_3 and the O_4 atoms, respectively. Moreover, the nonbonding orbitals (the 16th and 15th MOs of A) are combined to give localized spin orbitals on the $O_3$2py and the $O_4$2py orbitals, respectively. By combination of these localized orbitals, the 14th MOs of B are produced as

$$0.33\ O_3\text{2py} - 0.39\ O_3\text{2pz} \quad (1)$$

$$0.39\ O_4\text{2pz} - 0.26\ O_4\text{2py} - 0.20\ O_4\text{2px} \quad (2)$$

for the α- and the β-spin orbitals, respectively. Here the coefficients for the C_1 and the C_2 atomic orbitals (AO) are omitted for brevity. The 16th and 15th MOs are less polarized; accordingly, the origin of the biradical in the transition state B is attributed to the 14th MOs (1 and 2), which are the mixed σ and nonbonding orbitals.

Along the reaction path B to K_1, the energy of the singlet biradical decreases as the torsional angle τ, $\tau = \angle\ O_4$−C_2−C_1−O_3 increases from 28° to 68° (Table 3). A more detailed inspection of the potential energy curve is shown in the inset of Figure 3. The first minimum point along the flat potential is found at K_1, a small barrier was found at G_1, and the second minimum is found at K_2. The point G_1 is the transition state between the points K_1 and K_2. The reactant keeps the biradical spin states on the reaction path B → D_1 as shown in Figure 5.

At the points A and B, two nonbonding orbitals are doubly occupied. At the point G_1, one of the nonbonding orbitals is vacant and a couple of electrons are moved to the σ^* orbitals (15th MO). The σ orbital (14th MO) of A is going to the π or π^* orbitals of the formaldehyde molecule after the dissociation; accordingly, we will call the σ orbital a π or π^* orbital hereafter. The 14th spin orbitals of G_1 are the nonbonding orbitals of the O_3 and the O_4, which are completely polarized (Figure 2). The 16th spin orbitals are π^* type on both the C_1−O_3 and C_2−O_4 bonds and are partly polarized. By filling the 16th and the 14th MOs of G_1, the electron configuration leading to the $n\pi^*$ excited states of formaldehyde is appearing on both sides of DO. If the C_1−C_2 breaking proceeds keeping the electron configuration, two formaldehyde molecules will be formed in the $n\pi^*$ excited state. The 15th MOs of G_1 (σ^* type mentioned above) are regarded as the π(C−O) type partly polarized on both of the C−O bonds. Inspection of these MOs show that chemogenesis of the $n\pi^*$ excited states (S_1) is emerging on both of the C−O bonds, because two of four nonbonding electrons in A and B are brought to the π^* orbitals (the 16th MOs). Actually, DO on the point G_1 decays to the ground state unless enough energy is given; however, it has a chance of being raised to the S_1 state if the energy is supplied through this passage. The main route of deactivation is G_1 → K_2 → D_1 → F; the molecule loses the energy by radiationless transition and dissociates to two formaldehyde molecules.

At the point D_1, the nonbonding orbitals ($O_3$2py and $O_4$2px) mix with the π orbitals; this point is a junction to the S_1 and the S_0 state. Two formaldehyde molecules in the ground state (F) are formed by the C_1−C_2 bond breaking, unless more energy is supplied at the point D_1.

The trans isomer of the singlet biradical (K_3) is obtained by internal rotation from the point K_2 through the potential barrier of 0.87 kcal/mol at the point P_1, as shown in Scheme 1 and in the inset of Figure 4. Because the barrier height is too low, the trans form will be easily formed and dissociate exothermally through the minimum (K_3) and the edge (D_2) to two formaldehyde molecules in the ground state (F).

Small energy barriers are found on the potential surfaces of the biradical. To confirm the accuracy of calculation, we have calculated energies of these points by the uB3P86 method, as shown in Table 6. Taking an origin of energy at the minimum K_1 in the S_0 surface, both methods give almost the same energy

TABLE 6: Comparison of Calculated Energies for Energy Minima and Transition States on the Reaction Path of Thermolysis of 1,2-Dioxetane into Two Formaldehyde Molecules using UB3P86/6-31+G(D)//UB3P86/6-31+G(D) and UB3LYP/6-31+G(D)//UB3LYP/6-31+G(D)

a. Ground State(S_0)

	species	min A	ts B	min K1	ts G1	min K2	ts D1	min F
UB3P86	total energy *E*							
	Hartree (−229. +)	−0.502016	−0.465299	−0.486095	−0.485974	−0.486295	−0.486169	−0.579447
	Δ*E* kcal/mol[a]	−9.99	13.05	0.0	0.08	−0.12	−0.05	−58.58
UB3LYP[b]	Δ*E* kcal/mol[a]	−6.80	13.41	0.0	0.03	−0.13	−0.02	−62.24

b. Triplet State(T_1)

	species	min J1	ts H1	min J2	ts Q2	min Z
UB3P86	total energy *E*					
	Hartree (−229. +)	−0.486641	−0.485902	−0.487251	−0.4703573	−0.4704359
	Δ*E* kcal/mol[a]	−0.34	0.12	−0.73	9.88	9.83
UB3LYP[b]	Δ*E* kcal/mol[a]	−0.29	0.09	−0.71	7.72	6.53

[a] Δ*E* is the relative value with reference to energy of K1. $\Delta E = E - E(\mathrm{K1})$. [b] The total energies *E* calculated by the UB3LYP method are listed in Table 3.

values at G_1, K_2, D_1, J_1, H_1, and J_2. However, at the initial state A or the transition state Q_2, energy values given by B3P86 are different from those given by B3LYP by 2 to 3 kcal/mol because the molecular structures in A and Q_2 are very different from those of biradical states.

In the final conformation F, two formaldehyde molecules are in an antiparallel arrangement on the same plane, which is stabilized by dipole−dipole interaction and hydrogen bonding between the hydrogen atoms of the C−H bonds and the O atoms of the carbonyl groups, as shown in Scheme 1.

(c) Chemiluminescence of DO. Chemiluminescence appears from either the triplet (T_1) or the singlet (S_1) excited states. The potential energy curves of the T_1 states are calculated from the saddle points Q_1 or Q_2 to the energy minimum points on both sides by the IRC program. In the region between the point B and the point G_1, the potential energies of the T_1 state are calculated with the same geometries of the S_0 state along the IRC curve, as shown in Figures 3 and 4. The S_0 and T_1 intersection is found near the point B. After the intersection, the T_1 curve is below the S_0 curve, as shown in the inset of Figure 3.

To find the process of formation of the T_1 state, we examine the MOs of the S_0/T_1 intersection point on the IRC curve, because the change of the spin state must be correlated with the changes in the electronic configuration and MOs. In the S_0 state at the intersection, the character of MOs is almost the same as that of B; therefore, we compare the MOs of B in the S_0 state and those of S_0/T_1 in the T_1 state (Figure 2) to find the orbital changed. We find that the 14th β spin MO of B (formula 2) is transformed to the 15th α spin MO of T_1, which is given by

$$0.29\ \mathrm{O_3(2py)} - 0.26\ \mathrm{O_4(2py)} + 0.20\ \mathrm{O_4(2pz)} - 0.11\ \mathrm{O_4(2px)} \quad (3)$$

This transition is associated with the orbital angular momentum changes at the O_4 orbitals associated with the transitions between the 2py → 2pz, the 2pz → 2px, and the 2px → 2py.

To transfer the S_0 to the T_1 state, the matrix element *V* of the spin−orbit (SO) coupling, or LS coupling, is important. It is now obvious that the matrix elements $<2py|L_x|2pz>$, $<2pz|L_y|2px>$, and $<2px|L_z|2py>$ are significant because of the presence of the AO coefficients of 2px, 2py, and 2pz at the O_4 in the 14th β MO of B in the S_0 state and the 15th α MO of S_0/T_1 in the T_1 state (formulas 2 and 3). The SO coupling energies were calculated with the conformation of the intersection (S_0/T_1) by the Gaussian CASSCF program; the energy is estimated to be as large as 1 cm^{-1}. This value is big enough to avoid crossing. Moreover, the geometry of the molecule is the same for the S_0 and the T_1 states at the S_0/T_1 intersection; accordingly, the one-dimensional Landau−Zener formula is applicable.

Nakamura and Zhu[30] presented a rigorous and approximate Landau−Zener[31,32] formula of the transition probability *p*. The approximate formula is as follows:

$$p = \exp\left[-\frac{2\pi V^2}{\hbar\nu|F_1 - F_2|}\right] = \exp\left[-\frac{\pi}{4\sqrt{\alpha\beta}}\right] \quad (4)$$

$$\alpha = \frac{\hbar^2\sqrt{|F_1 - F_2|}(F_1 - F_2)}{(16mV^3)} \quad (5)$$

$$\beta = \frac{(E - E_x)(F_1 - F_2)}{2\sqrt{|F_1 - F_2|V}} \quad (6)$$

where F_1 and F_2 are the slopes of two potential curves near the crossing point, E_x is the energy of the crossing point, and *m* is the reduced mass in the reaction coordinate. This formula is useful when the signs of slopes, F_1 and F_2, are the same. By estimating these values from Figure 3, and when *E* is taken close to E_x, the *p* value at the crossing point is found to be zero. This means that the singlet (S_0) to the triplet (T_1) intersystem crossing occurs completely at the crossing point.

After crossing, the T_1 and the S_0 curves are almost parallel, and the energies of the T_1 state are always less than the S_0 state, as shown in Figures 3 and 4 and Tables 3 and 4. The overview of potential surfaces is shown in Figures 6 and 7. The two potential curves coincide at the points G_1 and H_1, and the geometry of H_1 is exactly the same as that of point G_1 (Tables 3 and 4).

In this region where potential surfaces contact, the energy difference between the S_0 and the T_1 states is of the same order of magnitude as the thermal energy, k_BT; accordingly, the T_1/S_0 conversion occurs frequently, and the T_1 and S_0 states may coexist. The MOs at the point H_1 show that the 14th and the 15th α-spin MOs are symmetric and antisymmetric combinations, respectively, of the nonbonding orbitals of the $O_3$2py and the $O_4$2px orbitals (Figure 2). These orbitals are occupied by the α spin electrons giving the triplet state. In the G_1 state the nonbonding orbitals, the $O_3$2py and the $O_4$2px, are not coupled

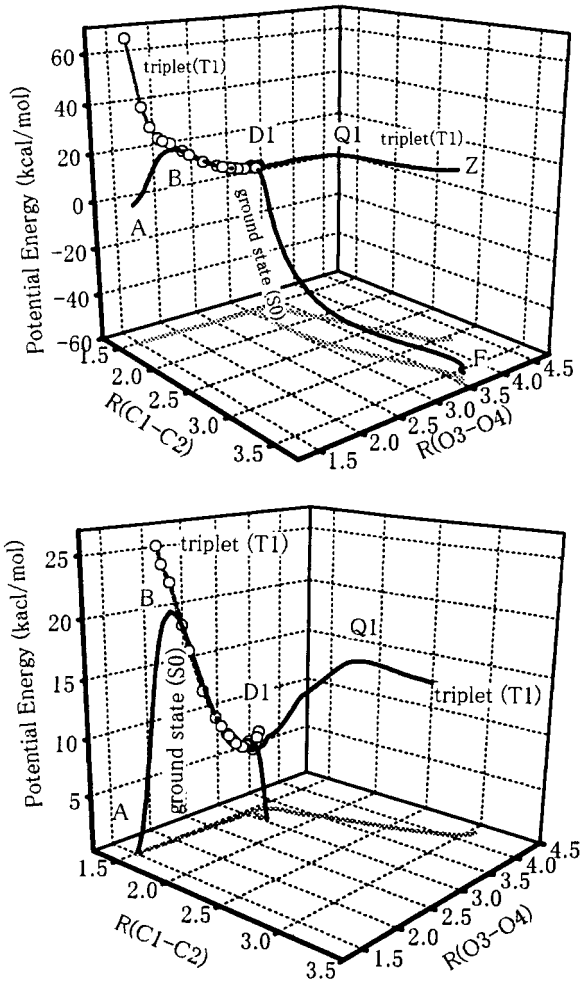

Figure 6. (a) The potential energy of the S_0 and the T_1 states of 1,2-dioxetane vs the bond distances of the C_1-C_2 and O_3-O_4 bonds (units in Å) along the gauche route. The projections of the potential curves on the *xy* plane show that the O_3-O_4 bond breaking occurs first and the C_1-C_2 bond rupture occurs subsequently. (b) The potential energy curves of Figure 6a are shown by expanded scale of *z* axis to compare with those of MCSCF/6-31G(d) shown in Figure 11.

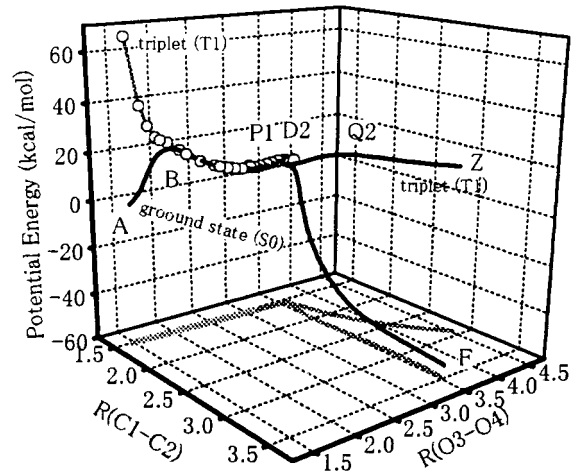

Figure 7. The potential energy of the S_0 and the T_1 states of 1,2-dioxetane vs the bond distances of the C_1-C_2 and O_3-O_4 bonds (units in Å) along the trans route. A small barrier P_1 is the barrier of the internal rotation to the trans conformer in the S_0 state. The projections of the potential curves, drawn on the *xy* plane, show that the O_3-O_4 bond rupture precedes the C_1-C_2 bond rupture.

and are singly occupied with antiparallel spin electrons. Actually, the orbital energies of the 14th MOs of G_1 and H_1 are the same, and the 15th MO of H_1 is only slightly (0.06 eV) higher; this means that these four orbitals are almost degenerate at these points.

At the point H_1, the $O_4$2px in the 14th α-MO is not coupled with the $O_4$2pz orbital. At the points J_1 and J_2, the $O_4$2pz mixes with the $O_4$2px MO in the 14th and 15th β MOs, in phase (J_2) and out of phase (J_1). The change in the sign of the coefficients of mixed orbitals correlates to the change of the electronic structure. At the point J_2, the biradical becomes the precursor of the $n\pi^*$ excited state. The torsional angle increased by 20°, from 66° at J_1 to 86° at J_2 (Table 3). In the earlier studies on MOs of dioxetanes, such electron configurations with singly occupied nonbonding orbitals were mentioned by Turro and Devaquet.[33]

From the energy minimum point J_2 to the saddle point Q_1, the C_1-C_2 bond length is increased from 1.555 to 2.286 Å. The MOs at Q_1 (Figure 2) show that the left side of DO is going to the ground state of formaldehyde and the right side is forming the $n\pi^*$ (T_1) state of formaldehyde. The potential energy at Q_1 is 9.07 kcal/mol higher relative to the J_2 (Figure 3, inset). In the final conformation, Z, the formaldehyde molecule in the T_1 state takes a nonplanar conformation (Scheme 1).

The overview of potential energy curves and their projections (Figures 6 and 7) shows that the O_3-O_4 bond breaking precedes the C_1-C_2 bond cleavage. These curves clearly indicate that the chemiluminescence occurs through the two steps of the bond rupture.

In the region where the C_1-C_2 bond begins to break near point D_1, the S_0 and the T_1 curves cross again; accordingly, the possibility of back transfer from $T_1 \rightarrow S_0$ is conceivable, although Turro and Devaquet[33] disregarded it. Quantitative estimate of the portion of back transfer is a difficult problem; therefore, we used experimental chemiluminescence yield to estimate the nonradiative rate of deactivation through the S_0 route in the last section.

The change of the spin population in the T_1 state is illustrated in Figure 5, where the generation of the T_1 state on one side of DO is clearly indicated. In the final minimum point Z, formaldehyde molecules in the S_0 and the T_1 states take face-to-face arrangement as shown in Scheme 1. The face-to-face arrangement of molecules indicates that a stacked structure is more stable; it implies that the triplet excimer is formed. In the ground state (F) the two formaldehyde molecules are bound by hydrogen bonding (Scheme 1). The yield of the T_1 state of DO is only 0.0024 (Table 1). This point will be discussed in the last section.

The trans conformer of T_1 is obtained by internal rotation from J_2 through a low potential barrier at P_2. It dissociates after overriding the barrier of 8.73 kcal at Q_2 to the T_1 and the S_0 fragments of formaldehyde molecules (Z). Because the association energy of Z is very small, they will easily decompose to the T_1 and the S_0 of formaldehyde molecules. A detail of the potential function is illustrated in the inset of Figure 4.

Comparing with the earlier MO calculation on the reaction path, we found that the semiempirical calculation of Wilson and Halpern[15] is closest to our result. Parallel potential curves of the singlet and the triplet biradicals were confirmed in both calculations, thus ruling out an asymmetric triplet state far below the potential barrier proposed by Turro and Devaquet.[33]

(d) Reaction Pathway of TMDO. TMDO is more stable than DO, and the yield of chemiluminescence is much higher than DO. Accordingly, more experimental results are reported on TMDO than on DO.[18,34−36] The energy minima and transition states of the S_0 and the T_1 states found along the reaction path

TABLE 7: Energies and Skeletal Part of Geometrical Parameters[a] for Energy Minima and Transition States along the Reaction Path of Thermolysis of 3,3,4,4-Tetramethyl-1,2-dioxetane into Two Acetone Molecules in the Ground State (S_0); uB3LYP/6-31+G(d)//uB3LYP/6-31+G(d)

species	ts 0	min A	ts B	min K1	min K2	ts D	F
total energy *E*							
Hartree (−386. +)	−0.216809	−0.217914	−0.181234	−0.192948	−0.194278	−0.193039	−0.337452
Δ*E* kcal/mol	0.69	0.00	23.02	15.67	14.83	15.61	−75.01
zero-point energy Hartree (ZPE)	0.173537	0.173882	0.170881	0.169583	0.170100	0.168571	0.168705
Δ(*E* + ZPE) kcal/mol	0.48	0.00	21.13	12.97	12.46	12.28	−78.26
r(C1−C2) Å	1.563	1.558	1.561	1.584	1.601	1.627	3.526
r(C1−O3) Å	1.469	1.471	1.432	1.382	1.368	1.363	1.222
r(C2−O4) Å	1.469	1.471	1.432	1.382	1.368	1.370	1.222
r(C1−C5) Å	1.526	1.528	1.533	1.545	1.567	1.545	1.516
r(C2−C6) Å	1.526	1.528	1.533	1.545	1.567	1.555	1.516
r(C1−C7) Å	1.526	1.521	1.536	1.562	1.544	1.566	1.516
r(C2−C8) Å	1.526	1.521	1.536	1.562	1.544	1.542	1.516
r(O3−O4) Å	1.485	1.488	2.052	2.843	2.891	2.910	3.562
∠C2−C1−O3	88.48	87.46	96.62	109.13	110.23	111.37	70.62
∠C1−C2−O4	88.48	87.46	96.62	109.09	110.26	105.27	70.62
∠C2−C1−C5	117.58	115.53	114.42	112.50	108.95	111.23	96.79
∠C1−C2−C6	117.58	115.57	114.38	112.51	108.96	109.69	101.83
∠C2−C1−C7	117.58	119.59	116.82	113.13	113.69	110.50	101.83
∠C1−C2−C8	117.58	119.57	116.82	113.19	113.62	113.42	96.79
∠O4−C2−C1−O3	0.00	−16.39	−32.50	−63.57	−64.24	−71.59	−180.00
∠C5−C1(C2)−O3	111.88	110.18	115.19	121.36	112.54	123.36	121.13
∠C6−C2(C1)−O4	111.88	110.16	115.19	121.33	112.52	113.73	119.60
∠C7−C1(C2)−O3	−111.88	−112.54	−113.28	−114.32	−125.00	−114.49	−119.60
∠C8−C2(C1)−O4	−111.88	−112.55	−113.26	−114.28	−125.10	−122.13	−121.13

[a] ∠p-q-(r)-s represents the dihedral angle between the plane(p-q-r) and the plane(s-q-r). The unit of angle is degree.

are listed in Tables 7 and 8. The stable structure of TMDO is shown in Figure 1. The overview of the potential energy curve of the S_0 state shown in Figure 8 is similar in shape to that for DO. The calculated dissociation energy is 23 kcal/mole, which is larger than for DO, in agreement with experimental trend shown in Table 5. uB3P86 gives larger dissociation energies, in better agreement with the experimental activation energies (Table 5).

The most remarkable result of TMDO is that the barrier for the dissociation of the C_1-C_2 bond is almost zero. It implies that the T_1 state is easily produced after the O_3-O_4 bond breaking, and that therefore a high quantum yield of chemiluminescence (Table 1) is reasonable. Because the total energy of two fragments, where one of acetone is in the triplet state (a + a*), has lower energy than the energy at Q_1, the reaction from the biradical to the fragments is exothermic. Accordingly, the triplet state of acetone (a*) will be easily populated by thermal decomposition of the intermediate at Q_1.

The X band of TMDO, which was found by Cannon and Crim[19] and studied by Haas et al.,[20,21] transiently appears immediately after the laser excitation at the blue side of acetone phosophorescence. To investigate further the origin of the X band, the dissociation curve is followed along the C_1-C_2 distance from the minimum point Z_1 ($C_1-C_2 = 4.06$ Å) to 14 Å, keeping other geometrical parameters fixed. The potental energy curve is shown in Figure 9 and the geometrical structure at the point Z_1 is shown in Figure 10. Similarly, along the trans route, the minimum point is found at Z_2, whose structure is shown in Figure 10. The structures for the points Z_1 and Z_2 are a kind of excimer, because two acetone molecules are bound together and one is in the triplet excited state. For comparison, the stable conformation of the acetone dimer in the ground state is also illustrated in Figure 10.

Cannon and Crim[19] and Haas et al.[21b] once mentioned the possibility of an excimer for the X band. In the later work, Haas et al.[21a] have interpreted the X band as vibrationally excited acetone in a mixed singlet and triplet $n\pi^*$ state. However, an intermediate spin state with a different lifetime is unlikely. The lifetime of the X band is about 50 μs at reduced pressure,[19] representing collisional quenching, which is close to acetone triplet (170 μs[37]) rather than singlet (few *ns*).[38] It is more likely that the X band is due to the triplet state of hitherto unknown species. An intermediate state in the shallow minima at Z_1 may be responsible for it. The emission occurs from the triplet to the singlet state vertically, and the energy difference between the two potential curves corresponds to the X band. The vertical transition energy between the point Z_1 and the ground state is 17 700 cm^{-1}, while the value for free acetone is 17 400 cm^{-1}. In the experiment, the blueshift is about 1700 cm^{-1}, the X band appeared at 23 800 cm^{-1}, and the phosophorescence of acetone is at 22 100 cm^{-1}; accordingly, the calculated result is semiquantitatively in agreement with the experiment showing the blueshift.

The calculations on the stabilization energies of the dimers and the excimers of formaldehyde and acetone are summarized in Table 9. The ground state dimers show much larger dimerization energies than the excimers, but the values of the excimers are substantial enough to be detected in favorable conditions.

Finally, heat of dissociation of 1,2-dioxetane is calculated by B3LYP, B3P86, and G2 theory as shown in Table 10. The results are in good agreement with thermochemical estimates with deviation less than 6 kcal/mol. For DO B3LYP/6-31+G(d) and G2 theory gave the same results, which are in better agreement with thermochemical data than B3P86/6-31+G(d). For TMDO, B3P86/6-31+G(d) gave better results.

4.2. MCSCF Calculation of the Excited States of DO. To study the mechanism of the S_1 excited state being formed, an MCSCF calculation was performed for the S_0, S_1, and T_1 states of DO along the reaction path. The calculation covered the whole reaction path for comparison with the earlier results of Reguero et al.[14] They used eight electrons in the six orbitals for the configuration interaction (CI) (8, 6), two nonbonding orbitals ($O_3$2py, $O_4$2py) and four π type orbitals in the dissociated formaldehyde (O_3, O_4 2pz and C_1, C_2 2pz) of the

TABLE 8: Energies and Skeletal Part of Geometrical Parameters[a] for Energy Minima and Transition States along the Reaction Path of the Thermolysis of 3,3,4,4-Tetramethyl-1,2-dioxetane into Two Acetone Molecules in the Triplet State (T_1); uB3LYP/6-31+G(d)//uB3LYP/6-31+G(d)

species	min J1	ts H	min J2	ts Q1	Z1	ts P	min J3	ts Q2	Z2
total energy *E*									
Hartree (−386. +)	−0.194767	−0.194137	−0.194396	−0.193353	−0.215604	−0.190023	−0.200357	−0.199521	−0.215419
Δ*E* kcal/mol	14.52	14.92	14.76	15.41	1.45	17.50	11.02	11.54	1.57
zero-point energy Hartree (ZPE)	0.170211	0.169066	0.169533	0.168370	0.166189	0.169559	0.169531	0.168377	0.166237
Δ(*E* + ZPE) kcal/mol	12.22	11.90	12.03	11.95	−3.38	14.79	8.29	8.09	−3.19
r(C1−C2) Å	1.602	1.642	1.691	1.907	4.056	1.765	1.717	1.923	4.006
r(C1−O3) Å	1.367	1.359	1.344	1.292	1.221	1.333	1.333	1.290	1.221
r(C2−O4) Å	1.367	1.354	1.345	1.314	1.326	1.331	1.335	1.310	1.326
r(C1−C5) Å	1.566	1.555	1.545	1.539	1.517	1.541	1.544	1.539	1.517
r(C2−C6) Å	1.567	1.565	1.557	1.547	1.524	1.567	1.556	1.548	1.525
r(C1−C7) Å	1.545	1.543	1.546	1.543	1.517	1.545	1.543	1.539	1.517
r(C2−C8) Å	1.545	1.550	1.557	1.550	1.523	1.554	1.555	1.548	1.525
r(O3−O4) Å	2.888	2.898	2.912	2.973	3.614	3.307	3.557	3.619	3.657
∠C2−C1−O3	110.05	105.45	102.30	99.52	78.42	102.86	103.40	101.69	70.11
∠C1−C2−O4	110.08	111.09	110.68	107.51	49.48	110.65	109.72	109.30	57.24
∠C2−C1−C5	109.00	107.79	107.69	103.77	104.12	106.49	107.18	102.97	99.89
∠C1−C2−C6	109.01	109.97	110.79	107.47	81.80	110.24	110.02	106.38	85.99
∠C2−C1−C7	113.70	112.55	110.79	106.90	87.26	110.85	107.13	102.97	99.89
∠C1−C2−C8	113.64	111.64	110.17	108.56	159.40	111.40	109.97	106.38	85.99
∠O4−C2−C1−O3	−64.69	−70.24	−75.27	−77.55	−142.53	−113.52	180.0	180.0	180.0
∠C5−C1(C2)−O3	112.76	115.05	117.89	119.62	120.01	119.02	120.39	121.37	120.21
∠C6−C2(C1)−O4	112.75	115.29	118.92	119.13	130.33	116.90	119.63	120.17	120.96
∠C7−C1(C2)−O3	−124.76	−122.28	−119.61	−120.19	−123.01	−119.66	−120.36	−121.37	−120.21
∠C8−C2(C1)−O4	−124.86	−122.98	−119.48	−119.11	−35.84	−121.65	−119.63	−120.17	−120.96

[a] ∠ p-q(r)-s represents the dihedral angle between the plane(p-q-r) and the plane(s-q-r). The unit of angle is degree.

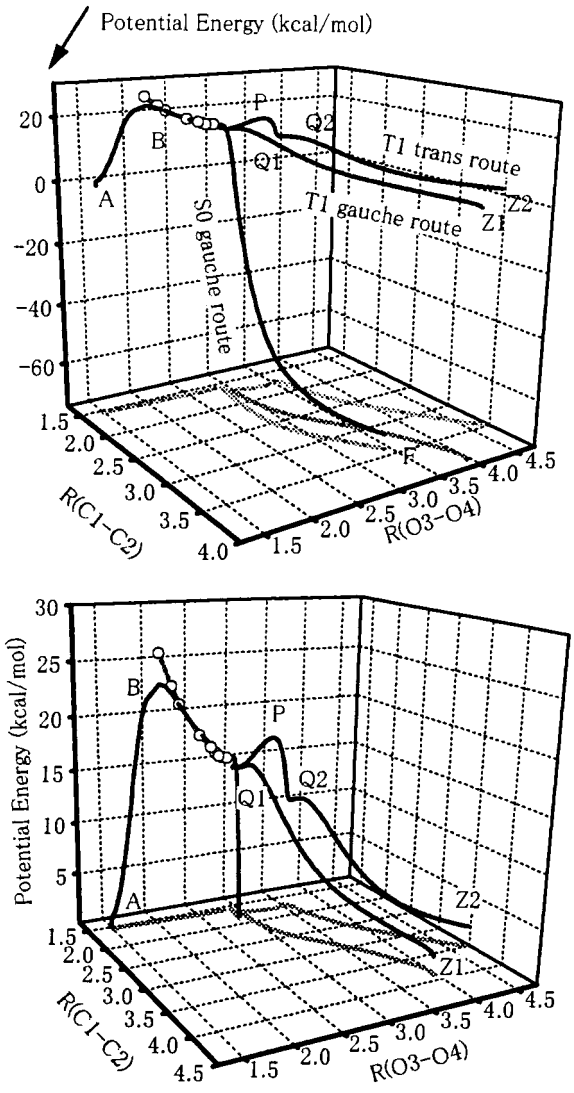

Figure 8. (a) Potential energy for the decomposition of 3,3,4,4-tetramethyl-1,2-dioxetane to two acetone molecules vs the bond distances of the C_1-C_2 and O_3-O_4 bonds (units in Å). The projections of the IRC curves indicate that the O_3-O_4 bond rupture precedes the C_1-C_2 bond rupture. P is a small barrier of the internal rotation in the trans route in the T_1 state. The Z1 and Z2 are the potential minima of the excimer of the gauche and the trans routes, respectively. The geometries of the Z1 and Z2 are shown in Figure 9. (b) Potential energy curves of Figure 8a are shown by expanded scale of *z* axis to compare with those of unsubstituted 1,2-dioxetane shown in Figure 6b.

C_1-C_2 and the O_3-O_4 bonds. We have referred to their reported structures to start the calculation.

To improve the numerical results, the 6-31G(d) basis is used and the size of the active space is expanded to (12, 8). A large active space is necessary for the IRC calculation connecting two different states, where more orbitals are involved in the conversion process from one configuration to the other. The choice of orbitals is important, and the orbtials participating in bond deformation or breaking should be included. At point A, the O2s orbitals included in the active space are effective, but at point B, the contribution of O2s is comparable to the O2px and the O2py orbitals.

In the previous MCSCF calculation, the potential barrier for the O_3-O_4 bond breaking was too low, while the barrier for the C_1-C_2 bond cleavage was too high. With the use of the 6-31G(d) basis, the energies and the optimized structures are improved to some extent; however, the potential barrier for the

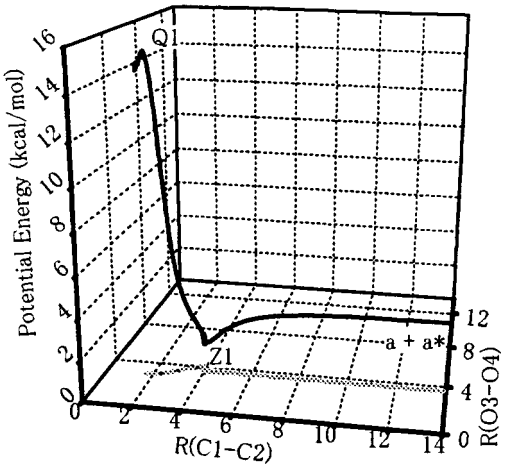

Figure 9. The potential energy curve of the decomposition of 3,3,4,4-tetramethyl-1,2-dioxetane(T_1) to two acetone molecules (one is in the S_0 state and the other is in the T_1 state) along the gauche route. The minimum point Z1 is an excimer state (Table 8) whose structure is shown in Figure 10. The energy at the end of the C_1-C_2 bond elongation is shown by the symbol (a + a*). Potential energies are given by relative values to the point A.

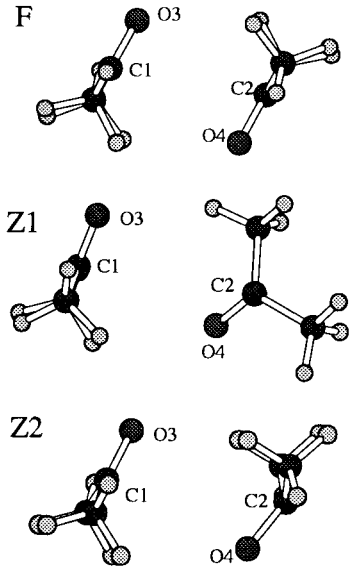

Figure 10. Geometrical structures of the dimer of acetone in the ground state (F) and in the excimer state in the gauche route (Z1) and the trans route (Z2). The distances of atomic contact are $C_1-C_2 = 3.526$, $C_1-O_4 = 3.326$, and $C_2-O_3 = 3.326$ Å at F; $C_1-C_2 = 4.056$, $C_1-O_4 = 3.350$ and $C_2-O_3 = 3.994$ Å at Z1; and $C_1-C_2 = 4.006$, $C_1-O_4 = 3.472$, and $C_2-O_3 = 3.770$ Å at Z2, respectively.

O_3-O_4 bond breaking is only 9.2 kcal/mol, which is certainly better than the previous value of 2.6 kcal/mol, but still too low compared to the 20.2 kcal/mol obtained by the uB3LYP method.

The S_0 potential curve is calculated by the IRC method from B to A and B to the minimum (K) of the S_0 curve, which is found at the torsional angle of $\tau = 66.9°$. The calculated energies for various states are shown in Table 11. The potential energy curves for the T_1 and the S_1 states in the region from A to K are calculated with the same geometries of the S_0 states as shown in Figures 11 and 12, where the overview of the potential curves for the gauche and the trans routes, respectively, are illustrated. These curves differ by the presence of a small barrier for the internal rotation from the gauche to the trans form at P in Figure 12. The S_0 and T_1 curves contact after the O_3-O_4 bond breaking at the S_0/T_1 conical intersection shown by a large white square in Figures 11 and 12, which is at $\tau = 57.6°$ near the bottom of the S_0 and the T_1 potential curves. The energy minimum, *J*, of the T_1 state is found at $\tau = 66.5°$, which is almost the same as the minimum K in the S_0 state found at $\tau = 66.9°$. The S_0/S_1 conical intersection is found at $\tau = 74.8°$, as shown by a large gray circle in Figures 11 and 12; the energy at this point is only 2.4 kcal/mol higher than the energy at K. Accordingly, the S_1 state will be populated thermally through the S_1/S_0 intersection.

The potential curves for the C_1-C_2 bond rupture are calculated by the IRC method using the CASSCF (12, 8) calculation for the T_1 and S_1 states. The height of the potential barrier for the T_1 state is calculated as 20.2 kcal/mol for the gauche and 18.8 kcal/mol for the trans routes, respectively, which are too high compared to the values of the uB3LYP method, 9.1 and 8.7 kcal/mol for the gauche and the trans routes, respectively. The potential barriers for the C_1-C_2 bond rupture in the S_1 state are calculated relative to K as 24.7 kcal/mol and 23.5 kcal/mol for the gauche and trans routes, respectively (Table 11).

Inspection of the CAS MOs (Figure 13) shows similarities with the uB3LYP results (Figure 2). In the potential energy minimum of the S_0 curve, K, the 17th and the 16th MOs are singly occupied with antiparallel spin electrons. These MOs are composed of the nonbonding orbitals described by

$$O_3 2py \pm O_4(2px + 2py) \qquad (7)$$

At the minimum points of the T_1, J, the 16th and the 17th MOs are $O_3 2py$ and $O_4(2px + 2py)$ and are singly occupied.

The MOs at the S_0/T_1 intersection are almost the same as those of the K for both the S_0 and the T_1 states. In the S_0 at S_0/T_1, the 16th and 17th MOs are occupied by antiparallel spin electrons, while in the T_1 at S_0/T_1, they are filled with parallel spin electrons.

At the S_0/S_1 intersection, the electron configuration of the two states is different in the occupancy of the 15th and 16th MOs. In the S_0, the 15th MO is singly and the 16th MO is doubly occupied, and in the S_1 state, the 15th is doubly and the 16th is singly occupied, while the 17th MO is singly occupied in both states. The transformation of the $S_0 \rightarrow S_1$ occurred in the changes of occupancy of the $O_4 2px - O_4 2pz$ orbital to the $O_4 2px + O_4 2pz$ orbital. Emergence of the S_1 excited state is correlated to the change of the electron configuration at the O_4 nonbonding and the π^* orbitals. At the potential maxima Q, the 16th and the 17th MOs are singly occupied with the antiparallel spin electrons in the S_1 and with the parallel spin electrons in the T_1 state, respectively (Figure 13). The electron configuration demonstrates that the $n\pi^*$ excited state is prepared on the right side of the carbonyl group of DO at the saddle point Q.

Quite recently, Wilsey et al.[39] have presented extensive calculations on DO by using CASSCF (MCSCF) with MP2 correction to improve exploratory work.[14] The deficient barrier for O−O bond breaking is improved from 3 to 16 kcal/mol with MP2 correction; however, the potential surfaces of biradical, S_0 and T_1, are separated by 3 to 6 kcal/mol. The T_1 is higher in energy than the S_0 for all points in the biradical region; this is not consistent with Hund's rule for open-shell systems. By the uB3LYP method, most of the T_1 states in the biradical region are lower in energy than S_0 state, consistent with Hund's rule.

The present MCSCF calculation shows the energies of the S_1 and T_1 states and the change of occupancies in the MOs of biradical at the T_1/S_0 and S_1/S_0 intersections. The sequence of MOs is changed accompanying conformational changes, and the excited states of fragments are produced after the dissociation

TABLE 9: Total Energies of Monomers, Dimers, and Excimers of Formaldehyde and Acetone; uB3LYP/6-31+G(d)//uB3LYP/6-31+G(d)

	formaldehyde		acetone		
monomer	f (S_0 state)	f* (T_1 state)	a (S_0 state)	a* (T_1 state)	
total energy *E* (Hartree)	−114.508839	−114.400882	−193.166253	−193.046304	
two monomers	f + f	f + f*	a + a	a + a*	
total energy *E* (Hartree)	−229.017678	−228.909721	−386.332506	−386.212557	
dimers and excimers	dimer (F)	excimer (Z)	dimer (F)	excimer (Z1)	excimer (Z2)
total energy *E* (Hartree)	−229.021818	−228.912222	−386.337452	−386.215604	−386.215419
stabilization energy (kcal/mol)	2.60	1.57	3.10	1.91	1.80

TABLE 10: ΔH_r of the Dissociation of 1,2-Dioxetanes to Carbonyl Compounds

	B3LYP[a]	B3P86[b]	G2MP2	thermochemical calc.
		Sum of Electronic and Thermal Enthalpies		
DO	−228.866370 Hartree	−229.434519 Hartree	−228.574175 Hartree	
formaldehyde	−114.478272	−114.757006	−114.332262	
ΔH_r	−56.59 kcal/mol	−49.88 kcal/mol	−56.69 kcal/mol	−55.4 kcal/mol[4a,4b]
		Sum of Electronic and Thermal Enthalpies		
TMDO	−386.033855 Hartree	−387.189219 Hartree		
acetone	−193.076026	−193.647862		
ΔH_r	−74.17 kcal/mol	−66.88 kcal/mol		−68.35 kcal/mol[4a,4b]

[a] B3LYP/6-31+G(d)//B3LYP/6-31+G(d). [b] B3P86/6-31+G(d)//B3P86/6-31+G(d).

TABLE 11: Energies and Skeletal Part of Geometrical Parameters[a] for Energy Minima and Transition States along the Reaction Path of Thermolysis of 1,2-Dioxetane into Two Formaldehyde Molecules Calculated by CASSCF(12,8)/6-31G(d)//CASSCF(12,8)/6-31G(d)

	S_0			conical intersections		T_1 gauche	T_1 gauche	S_1 gauche	T_1 trans	S_1 trans
species	min A	ts B	min K	S_0/T_1	S_0/S_1	min J	ts Q(T_1)	ts Q(S_1)	ts Q(T_1)	ts Q(S_1)
total energy										
Hartree (−227. +)	−0.701673	−0.687031	−0.698409	−0.697594	−0.694528	−0.698147	−0.665959	−0.659111	−0.668158	−0.660993
ΔE kcal/mol	0.0	9.19	2.05	2.56	4.48	2.21	22.41	26.71	21.03	25.53
zero-point energy Hartree (ZPE)	0.066044	0.064282	0.061986			0.061708	0.058831	0.058824	0.058925	0.058797
$\Delta(E + ZPE)$ kcal/mol	0.0	8.08	−0.50			−0.51	17.88	22.18	16.56	20.98
r(C1−C2) Å	1.538	1.534	1.547	1.550	1.561	1.547	2.037	2.091	2.033	2.084
r(C1−O3) Å	1.423	1.409	1.384	1.381	1.379	1.384	1.251	1.246	1.252	1.246
r(C2−O4) Å	1.423	1.409	1.384	1.381	1.384	1.385	1.335	1.346	1.336	1.348
r(O3−O4) Å	1.551	2.146	2.961	2.898	2.980	2.964	3.261	3.273	3.729	3.762
∠C2−C1−O3	89.89	99.13	112.44	112.93	113.47	112.63	104.66	103.77	103.87	104.11
∠C1−C2−O4	89.89	99.12	112.45	112.91	107.80	112.61	112.02	110.86	110.21	109.02
∠O4−C2−C1−O3	−9.53	−34.49	−66.89	−57.64	−74.84	−66.45	−80.23	−79.45	180.02	179.96

[a] The unit of angle is degree. Energies in kcal/mol relative to the minimum A(S_0).

TABLE 12: Reaction Rate Constants of Thermolysis of 1,2-Dioxetane and 3,3,4,4-Tetramethyl-1,2-dioxetane

		ΔE kcal/mol	$\Delta(E + ZPE)$ kcal/mol	k (333 K) s^{-1}	k_{DO}/k_{TMDO}
experimental[18]	DO		22.7	9.71×10^{-3}	
	TMDO		27.8	7.3×10^{-5}	1.33×10^{2}
best fit	DO	24.79	22.47	9.71×10^{-3}	
	TMDO	27.57	25.69	7.31×10^{-5}	1.33×10^{2}
uB3P86[a]	DO	23.04	20.72	1.37×10^{-1}	
	TMDO	25.81	23.93	1.05×10^{-3}	1.30×10^{2}
uB3LYP[b]	DO	20.21	17.89	9.84	
	TMDO	23.02	21.13	7.08×10^{-2}	1.39×10^{2}

[a] uB3p86/6-31+G(d)//uB3P86/6-31+G(d). [b] uB3LYP/6-31+G(d)//uB3LYP/6-31+G(d).

of C_1-C_2 bond. The mechanism of chemogenesis is clarified on the basis of electronic configurations of DOs during the O−O and C−C bond cleavage and reorganization to two carbonyl compounds.

4.3. RRKM Theory Applied to the Unimolecular Decomposition of Dioxetanes. The reaction rates of thermal decomposition are extensively studied by Adam and Baader[18] experimentally, and the activation energies and frequency factors are tabulated. Thermolyses of DOs are typical unimolecular reactions; RRKM theory is very efficient to analyze the reaction rate. Cannon and Crim[19] already used RRKM theory to calculate the energy-dependent reaction rate $k(E)$ on the laser photolysis of TMDO. In this section we will calculate the reaction rate of thermal decomposition from point A to point B and estimate chemiluminescence yield by finding the rate at point Q with the RRKM theory.

According to the RRKM theory, the unimolecular decomposition is given by

$$k(T) = \frac{e^{-E_0/k_BT}}{hQ}\int_0^E G^{\ddagger}(E^{\ddagger})e^{-E^{\ddagger}/k_BT}\,dE^{\ddagger} \qquad (8)$$

where Q is the partition function of the initial state, and $G^{\ddagger}(E^{\ddagger})$ is the sum over states for the energy range of $0 \sim E^{\ddagger}$ in the transition state. The Eyring formula is derived by using the partition function of the transition state $Q^{\ddagger}$, which is obtained

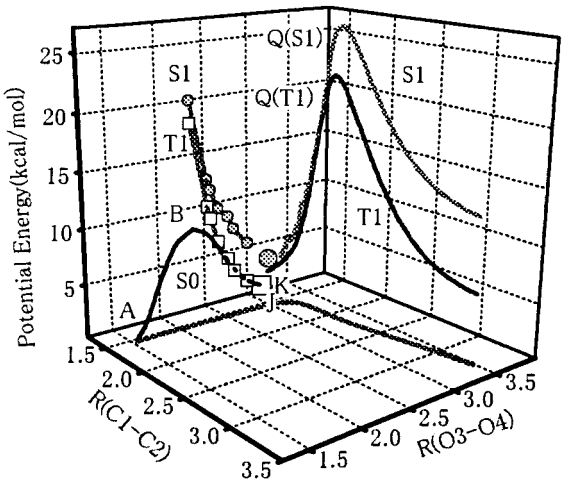

Figure 11. Potential energy curves calculated by the MCSCF for the decomposition of 1,2-dioxetane to two formaldehyde molecules through the gauche route. One of the produced formaldehyde molecules is in either the T_1 or the S_1 excited state. The S_0/T_1 conical intersection is shown by a large white square and the S_0/S_1 conical intersection is shown by a large gray circle. The small white squares are calculated energies of the T_1 state with the geometries of the S_0 state, and the small gray circles are those of the S_1 state with the geometries of the S_0 state. Potential energies are given by relative values to the point A. Unit of bond length is Å.

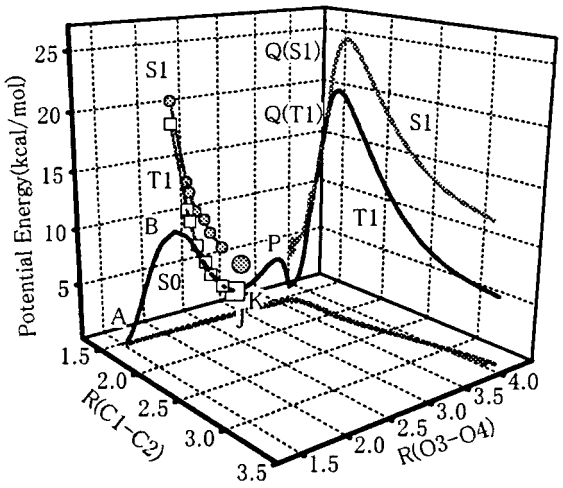

Figure 12. Potential energy curves calculated by the MCSCF for the decomposition of 1,2-dioxetane to two formaldehyde molecules through the trans route. A small barrier P near the S_0/T_1 conical intersection is the barrier for the internal rotation from the gauche to the trans conformer in the S_0 state. One of the produced formaldehyde molecules is in either the T_1 or the S_1 excited state. The S_0/T_1 conical intersection is shown by a large white square and the S_0/S_1 conical intersection is shown by a large gray circle. The small white squares are calculated energies of the T_1 state with the geometries of the S_0 state, and the small gray circles are those of the S_1 state with the geometries of the S_0 state. Potential energies are given by relative values to the point A. Unit of bond length is Å.

by integration of the above integral to ∞.

$$k(T) = \frac{k_B T}{h}\frac{Q^{\ddagger}}{Q} e^{-E_o/k_B T} \tag{9}$$

where E_o is the energy difference between the initial and the transition state including the zero-point vibrational energy (ZPE) correction.

The vibrational partition functions are calculated with all vibrational frequencies in the initial and the transition states using the uB3LYP method. The prefactor of eq 9 is the

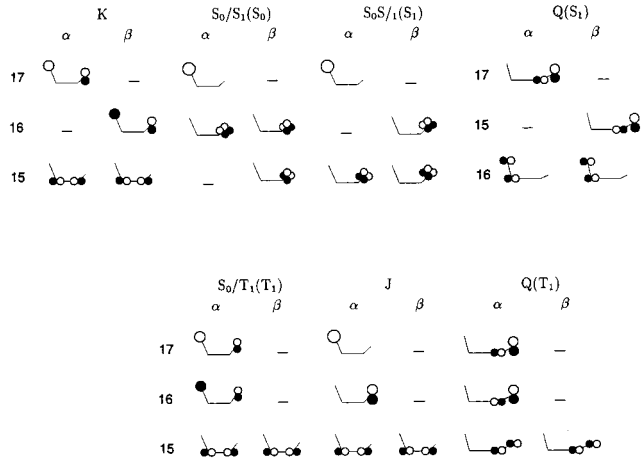

Figure 13. Change of MO along the reaction path leading to the excited state by the MCSCF calculation. K and J refer to the potential energy minima in the S_0 and T_1 states, respectively. $S_0/S_1(S_0)$ and $S_0/S_1(S_1)$ are the S_0 and S_1 states in the intersection, respectively. $S_0/T_1(T_1)$ is the T_1 state in the intersection. $Q(S_1)$ and $Q(T_1)$ are the transition states leading to the S_1 and the T_1 excited states of formaldehyde, respectively. All illustrations are projected onto the $O_3-C_1-C_2$ plane.

Arrhenius parameter. The calculated values are $\log_{10}A = 12.7$ for DO and TMDO, while reported values are 13.1 and 12.3 for DO and TMDO, respectively.[4] Because the rate is very sensitive to the activation energies, we estimate the activation energies to fit experimental rates as shown in Table 12. The difference between the calculated activation energies by the uB3P86 method with the best-fit values are only 1.7 kcal/mol (9% of ΔE), while the values by the uB3LYP method are 4.4 kcal/mol (18% of ΔE). The ratio of k(DO)/k(TMDO) is $\sim 1.3 \times 10^2$ for all calculated results. This implies that the present calculation explains the ratio of the reaction rates successfully, or, in other words, that the stability of TMDO compared to DO is calculated to a satisfactory level.

As regards the excited states, the chemiexcitation yields of DO and TMDO in the T_1 states are considered by calculating the rate for the C_1-C_2 bond cleavage along the $J_2 \rightarrow Q_1$. As mentioned in the previous sections, the potential barrier for the C_1-C_2 bond cleavage in TMDO is almost zero (0.65 kcal/mol), while the value for DO is about 9.07 kcal/mol. The rates of the C_1-C_2 bond breaking, $k_d(T_1)$, are calculated by the RRKM theory as 0.82×10^9 s^{-1} and 0.79×10^{13} s^{-1} for DO and TMDO, respectively. The nonradiative deactivation process, including the $T_1 \rightarrow S_0$ back transfer, competes with this process. Denoting the nonradiative rate as k_{nr}, and the rate of the C_1-C_2 bond breaking at the $J_2 \rightarrow Q_1$, as $k_d(T_1)$, and the dissociation to the S_1 state, $k_d(S_1)$, the experimental triplet emission yield η_t will be given by

$$\eta_t = \frac{3k_d(T_1)}{3k_d(T_1) + k_d(S_1) + k_{nr}} \tag{10}$$

where the value of $k_d(S_1)$ is negligible compared to other terms. The calculated rates $k_d(T_1)$ are multiplied by a factor of 3 of spin multiplicity. Using the values of triplet yield η_t shown in Table 1, the nonradiative rates are estimated as $k_{nr} = 1 \times 10^{12}$ s^{-1} for DO and $k_{nr} = 4.4 \times 10^{13}$ s^{-1} for TMDO, respectively. In view of the presence of many more vibrational modes in TMDO than DO, the larger value for TMDO is reasonable.

Finally, the branching ratio of S_1 and T_1 states, η_s/η_t, in the dissociation of DO is estimated by the ratio of rates, $k_d(T_1)$ and $k_d(S_1)$ calculated with MCSCF potential barriers and partition

functions as

$$\frac{\eta_s}{\eta_t} = \frac{k_d(S_1)}{3k_d(T_1)} \quad (11)$$

The calculated value is 0.0007, whereas the experimental ratio was 0.0013 (Table 1). The agreement is fairly satisfactory in view of the accuracy of the potential barrier calculation given in section 4.2.

5. Conclusion

Mechanisms of chemiluminescence of DO and TMDO are studied by Becke's three-parameter hybrid methods. Dissociation enthalpies of DO and TMDO to two carbonyl fragments calculated by uB3LYP/6-31+G(d) and uB3P86/6-31+G(d) are in reasonable agreement with thermochemical estimates. The O−O bond breakings of DO and TMDO are the rate-determining step of thermolysis, where activation energies of thermolysis calculated by these methods are in good agreement with experimental values. Stability of TMDO is more than 100 times larger than DO; this fact is well-explained by the rates of thermolysis calculated with RRKM theory. The rates of C−C bond rupture in the T_1 state are correlated to the triplet yield and radiationless transition rates of DO and TMDO. The higher triplet yield of TMDO compared to DO is well-explained by the potential barriers for the C−C bond rupture. The ratio of triplet to singlet yield of DO is discussed by the rates of C−C bond dissociation in the T_1 and S_1 states. Changes of molecular orbitals of DO along the reaction path are studied in detail, and the excitation mechanism is analyzed by the changes of electronic configuration.

These results demonstrate the utility of the uB3LYP and uB3P86 methods or the MCSCF method for calculating energies and geometries of dioxetanes in the S_0 and T_1, or the S_1 states, to a level of discussing the reaction rates and relative stabilities of reaction intermediates.

Acknowledgment. The authors thank Profs. M. Matsumoto, M. Ohashi, and Mr. H. Murayama of Kanagawa University for their kind suggestions, discussions, and help in computation. We also thank Profs. W. Adam of Würzburg University, T. Wilson of Harvard University, K. Yamaguchi of Osaka University, and H. Nakamura of the Institute for Molecular Science for kind discussions and sending information to us. We thank the computation center of the Institute for Molecular Science for the use of computers.

References and Notes

(1) (a) Wilson, T. *Int. Rev. Sci. Phys. Chem.* **1976**, *9*, 265. (b) Wilson, T. *Photochem. Photobiol.* **1995**, *62*, 601.

(2) Adam, W.; Cilento, G. *Angew. Chem., Int. Ed. Engl.* **1983**, *22*, 529.

(3) Adam, W.; Heil, M.; Mosandl, T.; Saha-Möller, C. R. In *Organic Peroxides*; Ando, W., Ed.; John Wiley and Sons: Chichester, 1992; p 252.

(4) (a) O'Neal, H. E.; Richardson, W. H. *J. Am. Chem. Soc.* **1970**, *92*, 6553. (b) O'Neal, H. E.; Richardson, W. H. *J. Am. Chem. Soc.* **1971**, *93*, 1828. (c) Richardson, W. H.; Yelvington, M. B.; O'Neal, H. E. *J. Am. Chem. Soc.* **1972**, *94*, 1619.

(5) Yamaguchi, K.; Fueno, T.; Fukutome, H. *Chem. Phys. Lett.* **1973**, *22*, 466.

(6) Evlet, E. M.; Feler, G. *Chem. Phys. Lett.* **1973**, *22*, 499.

(7) Harding, L. B.; Goddard, W. A., III. *J. Am. Chem. Soc.* **1977**, *99*, 4520.

(8) Horn, K. A.; Koo, J.; Schmidt, S. P.; Schuster, G. B. *Mol. Photochem.* **1978**, *9*, 1.

(9) McCapra, F. In *Bioluminescence and Chemiluminescence*; Hastings, J. W., Kricka, L. J., Stanley, P. E., Eds.; John Wiley and Sons: Chichester, 1996; p 7.

(10) Schaap, A. P.; Gagnon, S. D. *J. Am. Chem. Soc.* **1982**, *104*, 3504.

(11) (a) Matsumoto, M.; Suganuma, H.; Katao, Y.; Mutoh, H. *Chem. Commun.* **1995**, 431. (b) Matusmoto, M.; Arai, N.; Watanabe, N. *Tetrahedron Lett.* **1996**, *37*, 8535.

(12) Adam, W.; Bronstein, I.; Trofimov, A.V. *J. Phys. Chem. A* **1998**, *102*, 5406.

(13) Adam, W.; Bronstein, I.; Edwards, B.; Engel, T.; Reinhardt, D.; Schneider, F. W.; Trofimov, A. V.; Vasil'ev, R. F. *J. Am. Chem. Soc.* **1996**, *118*, 10400.

(14) Reguero, M.; Bernardi, F.; Bottoni, A.; Olivucci, M.; Robb, M. A. *J. Am. Chem. Soc.* **1991**, *113*, 1566.

(15) Wilson, T.; Halpern, A. M. *J. Phys. Org. Chem.* **1995**, *8*, 359.

(16) Vasil'ev, R. F. *J. Biolumin. Chemilumin.* **1998**, *13*, 69.

(17) Takano, Y.; Tsunesada, T.; Isobe, H.; Yoshioka, Y.; Yamaguchi, K.; Saito, I. *Bull. Chem. Soc. Jpn.* **1999**, *72*, 213.

(18) Adam, W.; Baader, W. J. *J. Am. Chem. Soc.* **1985**, *107*, 410.

(19) (a) Cannon, B. D.; Crim, F. F. *J. Chem. Phys.* **1980**, *73*, 3013. (b) Cannon, B. D.; Crim, F. F. *J. Chem. Phys.* **1981**, *75*, 1752. (c) Cannon, B. D.; Crim, F. F. *J. Am. Chem. Soc.* **1981**, *103*, 6722.

(20) Haas, Y. *Adv. Chem. Phys.* **1981**, *47*, 713.

(21) (a) Haas, Y.; Ruhman, S.; Greenblatt, G. D.; Anner, O. *J. Am. Chem. Soc.* **1985**, *107*, 5068. (b) Haas, Y.; Yahav, G. *Chem. Phys. Lett.* **1977**, *48*, 63.

(22) Becke, A. D. *J. Chem. Phys.* **1993**, *98*, 5648.

(23) Perdew, J. P. *Phys. Rev. B* **1986**, *33*, 8822.

(24) (a) Frisch, M. J.; Trucks, G. W.; Schlegel, H. B.; Gill, P. M. W.; Johnson, B. G.; Robb, M. A.; Cheeseman, J. R.; Keith, T.; Petersson, G. A.; Montgomery, J. A.; Raghavachari, K.; Al-Laham, M. A.; Zakrzewski, V. G.; Ortiz, J. V.; Foresman, J. B.; Cioslowski, J.; Stefanov, B. B.; Nanayakkara, A.; Challacombe, M.; Peng, C. Y.; Ayala, P. Y.; Chen, W.; Wong, M. W.; Andres, J. L.; Replogle, E. S.; Gomperts, R.; Martin, R. L.; Fox, D. J.; Binkley, J. S.; Defrees, D. J.; Baker, J.; Stewart, J. P.; Head-Gordon, M.; Gonzalez, C.; Pople, J. A. GAUSSIAN 94, Revision E.1; Gaussian, Inc: Pittsburgh, PA, 1995. (b) Frisch, M. J.; Trucks, G. W.; Schlegel, H. B.; Scuseria, G. E.; Robb, M. A.; Cheeseman, J. R.; Zakrzewski, V. G.; Montgomery, J. A., Jr.; Stratmann, R. E.; Burant, J. C.; Dapprich, S.; Millam, J. M.; Daniels, A. D.; Kudin, K. N.; Strain, M. C.; Farkas, O.; Tomasi, J.; Barone, V.; Cossi, M.; Cammi, R.; Mennucci, B.; Pomelli, C.; Adamo, C.; Clifford, S.; Ochterski, J.; Petersson, G. A.; Ayala, P. Y.; Cui, Q.; Morokuma, K.; Malick, D. K.; Rabuck, A. D.; Raghavachari, K.; Foresman, J. B.; Cioslowski, J.; Ortiz, J. V.; Stefanov, B. B.; Liu, G.; Liashenko, A.; Piskorz, P.; Komaromi, I.; Gomperts, R.; Martin, R. L.; Fox, D. J.; Keith, T.; Al-Laham, M. A.; Peng, C. Y.; Nanayakkara, A.; Gonzalez, C.; Challacombe, M.; Gill, P. M. W.; Johnson, B.; Chen, W.; Wong, M. W.; Andres, J. L.; Gonzalez, C.; Head-Gordon, M.; Replogle, E. S.; Pople, J. A. GAUSSIAN 98, Revision A.5; Gaussian, Inc.: Pittsburgh, PA, 1998.

(25) Gill, P. M. E.; Johnson, B. G.; Pople, J. A.; Frisch, M. J. *Int. J. Quantum Chem.* **1992**, *26*, 319.

(26) Curtiss, L. A.; Raghvachari, K. In *Computational Thermochemistry*; Irikura, K. K., Frurip, D. J., Eds.; American Chemical Society: Washington, DC, 1998; p 176.

(27) Politzer, P.; Seminario, J. M. In *Computational Thermochemistry*; Irikura, K. K., Frurip, D. J., Eds.; American Chemical Society: Washington, DC, 1998; p 359.

(28) Hess, J.; Vos, A. *Acta Crystallogr., Sect. B* **1977**, *33*, 3527.

(29) Matsumoto, M.; Watanabe, N.; Kasuga, N. C.; Hamada, F.; Tadokoro, K. *Tetrahedron Lett.* **1997**, 2863.

(30) Nakamura, H.; Zhu, C. *Comm. Mol. Phys.* **1996**, *32*, 249.

(31) Landau, L. D. *Phys. Zts. Sowiet.* **1932**, *2*, 46.

(32) Zener, C. *Proc. R. Soc. London, Ser. A*, **1932**, *137*, 696.

(33) Turro, N. J.; Devaquet, A. *J. Am. Chem. Soc.* **1975**, *97*, 3859.

(34) Simo, I.; Stauff, *J. Chem. Phys. Lett.* **1975**, *34*, 326.

(35) Brown, J. C.; Menzinger, M. *Chem. Phys. Lett.* **1978**, *54*, 235.

(36) Turro, N. J.; Lechtken, P.; Schore, N. E.; Schuster, G.; Steinmetzer, H. C.; Yekta, A. *Acc. Chem. Res.* **1974**, *7*, 97.

(37) Miller, J. C.; Borkmann, R. F. *J. Chem. Phys.* **1972**, *56*, 3727.

(38) Halpern, A. M.; Ware, W. R. *J. Chem. Phys.* **1971**, *54*, 1271.

(39) Wilsey, S.; Bernardi, F.; Olivucci, M.; Robb, M. A.; Murphy, S.; Adam, A. *J. Phys. Chem. A* **1999**, *103*, 1669.

(40) Hehre, W. J.; Radom, L.; Schleyer, P. v.R.; Pople, J. A. In *Ab Initio Molecular Orbital Theory*; John Wiley and Sons: New York, 1985, p 273.